



Eddy characteristics in the eastern South Pacific

Alexis Chaigneau, Oscar Pizarro

► To cite this version:

Alexis Chaigneau, Oscar Pizarro. Eddy characteristics in the eastern South Pacific. Journal of Geophysical Research, 2005, 110, pp.C06005, 12. 10.1029/2004JC002815 . hal-00123739

HAL Id: hal-00123739

<https://hal.science/hal-00123739>

Submitted on 11 Jun 2014

HAL is a multi-disciplinary open access archive for the deposit and dissemination of scientific research documents, whether they are published or not. The documents may come from teaching and research institutions in France or abroad, or from public or private research centers.

L'archive ouverte pluridisciplinaire **HAL**, est destinée au dépôt et à la diffusion de documents scientifiques de niveau recherche, publiés ou non, émanant des établissements d'enseignement et de recherche français ou étrangers, des laboratoires publics ou privés.

Correction published 19 August 2005

Eddy characteristics in the eastern South Pacific

Alexis Chaigneau

Centro de Investigación Oceanográfica en el Pacífico Sur-Oriental/Programa Regional de Oceanografía Física y Clima, Universidad de Concepción, Concepción, Chile

Oscar Pizarro

Departamento de Geofísica/Centro de Investigación Oceanográfica en el Pacífico Sur-Oriental/Programa Regional de Oceanografía Física y Clima, Universidad de Concepción, Concepción, Chile

Received 19 November 2004; revised 28 February 2005; accepted 17 March 2005; published 18 June 2005.

[1] The main eddy characteristics (length scales, rotation period, swirl and translation velocities) are determined in the eastern South Pacific region (10° – 35° S and 70° – 100° W) based on surface drifter measurements, satellite altimetry, and hydrographic data from the WOCE-P19 section. The “Chile-Peru Current eddies” have a typical diameter of order of 30 km, smaller than the typical Rossby radii observed in the region. They are principally formed near the South American coast and propagate seaward with a translation velocity varying from 3 cm s^{-1} in the southern part of the study domain to 6 cm s^{-1} north of 15° S. Long-lived anticyclonic eddies propagate northwestward with a mean angle of around 333° T, whereas cyclonic vortices propagate westward, consistent with the vortices propagation theory on a β plane. The radial distribution of the swirl velocity shows that the Chile-Peru Current eddies have a maximum diameter of order 200 km with a swirl velocity of around 14 cm s^{-1} and a rotation period of 50 days. Hydrographic data reveal a vertical extent down to around 2000 m for energetic eddies. No significant difference is observed between the tangential velocities of cyclonic and anticyclonic eddies. Geostrophic balance can be considered for large radii, whereas ageostrophic dynamics may play an important role near the eddy centers.

Citation: Chaigneau, A., and O. Pizarro (2005), Eddy characteristics in the eastern South Pacific, *J. Geophys. Res.*, **110**, C06005, doi:10.1029/2004JC002815.

1. Introduction

[2] During the last two decades, Lagrangian observations have been extensively used to study ocean surface characteristics from large-scale circulation to high-frequency tidal and inertial properties. However, these studies are principally limited to the Atlantic ocean [e.g., *Brugge*, 1995; *Martins et al.*, 2002] and the North Pacific [e.g., *Poulain and Niiler*, 1989; *Swenson and Niiler*, 1996], while there is a lack of knowledge on the surface ocean dynamics of the eastern South Pacific. Recently, *Chaigneau and Pizarro* [2005], have analyzed the large-scale circulation and turbulent flow characteristics of the study region (10° – 35° S and 70° – 100° W), based on 25 years of surface drifter measurements. This area includes the eastward South Pacific Current (SPC) south of 30° S which is part of the northeastern extension of the West Wind Drift [*Strub et al.*, 1998], the northward Chile-Peru Current (CPC) east of 82° W and the South Equatorial Current (SEC) flowing westward north of 25° S. The region is also known for the presence of a strong upwelling front, observed during summer and spring along the coast, separating relatively cold and fresh coastal water

from warmer and saltier offshore water [*Blanco et al.*, 2001].

[3] Superimposed on this large-scale circulation, the mesoscale turbulent flow shows typical Lagrangian time and length scales of around 3–6 days and 30–40 km respectively, with an elongation in the zonal direction [*Chaigneau and Pizarro*, 2005]. These length scales increase equatorward, proportionally to the Rossby radius, as observed from drifter measurements in the whole Pacific basin [*Zhurbas and Oh*, 2003, 2004] and from altimetry data [*Stammer*, 1997, 1998; *Chaigneau and Pizarro*, 2004]. Energetic mesoscale eddies have been observed in the region from both hydrographic data [*Blanco et al.*, 2001] and satellite measurements [*Hormazabal et al.*, 2004]. They have a clear signature on the eddy kinetic energy (EKE) calculated from altimeter measurements [*Hormazabal et al.*, 2004] and satellite tracked drifters [*Chaigneau and Pizarro*, 2005], with enhanced levels of EKE near the coast and in the southwestern part of the study domain. Mesoscale eddies play an important role in the ocean heat and freshwater transports [*Wunsch*, 1999; *Jayne and Marotzke*, 2002; *Zhurbas and Oh*, 2003, 2004]. Near the coast of the study region, *Chaigneau and Pizarro* [2005] have shown that in the surface layer, the lateral diffusion induced by the turbulent flow provides heat and salt to the coastal waters,

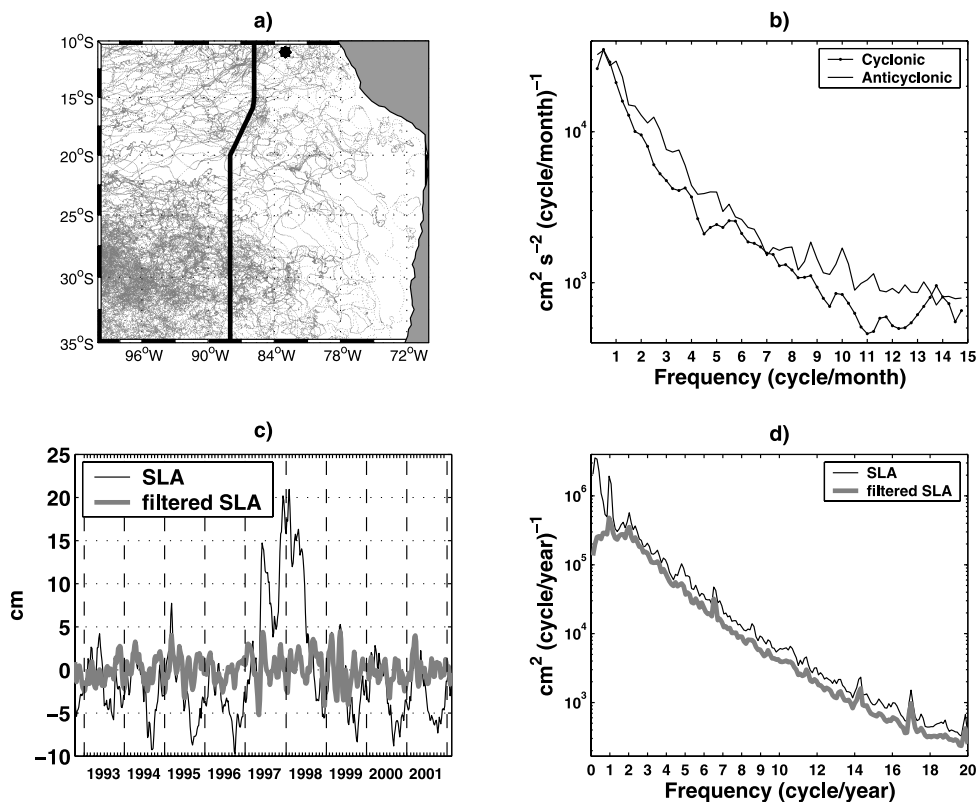


Figure 1. (a) Daily positions of the 476 surface drifters crossing the study region (70° – 100° W and 10° – 35° S) over the 1979–2003 period. The black line corresponds to the track of the WOCE-P19 section, whereas the black point is the geographic location of the sea level anomalies (SLA) shown in Figure 1c. (b) Mean rotary density spectrum obtained with the 160 drifter trajectories longer than 120 days. (c) Time series of the original SLA (thin line) and the filtered SLA (bold shaded line). (d) Spectrum of the original SLA (thin line) and the filtered SLA (bold shaded line).

and counterbalances totally the advective fluxes of the large-scale currents which transport relatively cold and fresh water from the south. However, the eddy characteristics in the eastern South Pacific have not been well documented. For example, what are their rotation periods? What are the corresponding diameters and swirl speeds? Do the cyclonic and anticyclonic eddies exhibit distinct characteristics? In order to validate numerical simulations of oceanic mesoscale features, it is important to have a good description of the eddy characteristics. This study will focus on the mesoscale characteristics of the eastern South Pacific based on satellite tracked drifter measurements, altimetry observations, and in situ hydrographic data.

[4] The paper is organized as follows. In section 2 we describe the data sets and the methods used to identify and characterize eddies. The horizontal characteristics and important eddy statistics are describe in section 3. In section 4, we study a particular cold core cyclonic eddy observed during a high-resolution hydrographic section. Finally, a discussion on the main results is given in section 5.

2. Data Sets and Methods

[5] The combination of different data sets, which provide distinct but complementary information, is necessary to describe eddy characteristics. For example, satellite tracked

drifters are useful to describe horizontal mesoscale features of several km and days. In contrast, altimetry measurements have typical resolutions of several tens km and weeks with a regular spatiotemporal coverage. Finally, hydrographic data are necessary to provide information on the eddy vertical structure.

[6] The surface satellite tracked drifter data set spans the period 1979–2003 and is part of the Global Drifter Program/Surface Velocity Program. In the study region a total of 476 different drifters were followed (Figure 1a). They were equipped with a holey sock drogue centered at 15 m depth in order to reduce surface drag induced by both wind and waves. The Atlantic Oceanographic and Meteorological Laboratory (AOML), Miami, received the drifter positions from Doppler measurements from Service ARGOS. These positions, irregularly distributed in time, were therefore quality controlled and interpolated to uniform 6 hour intervals using an optimum interpolation procedure [Hansen and Poulain, 1996]. Velocity components are calculated by a centered difference scheme at each 6 hour interval. Most of the drifters also provide surface temperature measurements, but due to the heterogeneity of the surface water in the study region, and the influence of the seasonal cycle on the surface temperature changes, we will not use these data. To remove high-frequency tidal and inertial wave energy and to avoid aliasing the energy into

the low-frequency motions, these drifter data were daily averaged [Swenson and Niiler, 1996; Martins *et al.*, 2002]. The maximum amount of data were observed during the 1990s, corresponding to the World Ocean Circulation Experiment (WOCE) period, and all seasons of the year were equally sampled. Figure 1a shows the spatial distribution of the daily data. There is higher resolution in the southwest and in the north of the study domain (10° – 35° S and 70° – 100° W), whereas the region near the coast is poorly sampled.

[7] Each trajectory was visually examined to extract all closed loops ascribed to the presence of vortex-like eddies. As a result, 1290 mesoscale current loops were obtained associated with eddies or vortices having a closed circulation; 35% of the total correspond to a cyclonic rotation and 65% to anticyclones. These complete vortices, which certainly correspond to the most energetic structures, are mostly observed in the southwest part of the domain (not shown) where the number of data is enhanced (Figure 1a).

[8] Figure 1b shows the mean rotary spectrum obtained with the 160 drifter trajectories longer than 120 days. It confirms that anticyclonic rotation dominates cyclonic rotation in all the frequency bands. Furthermore, the difference between cyclonic and anticyclonic spectrum energies is increased for displacement periods of 3–5 days (~ 8 – 13 cycles per month) corresponding to the shorter loops and typical Lagrangian timescales of the turbulent flow in the region [Chaigneau and Pizarro, 2005]. For lower frequencies, the large-scale circulation also indicates anticyclonic rotation enhanced by the large-scale gyre bounded by the eastward SPC south of 30° S, the equatorward CPC east of 82° S and the SEC flowing westward north of $\sim 25^{\circ}$ S [Chaigneau and Pizarro, 2005]. The following drifter results and statistics are thus based on the 1290 closed loops. For each complete loop, the rotation period, the mean position, diameter and tangential or swirl velocity were determined. The swirl velocity V_{θ} is obtained by $V_{\theta} = L/T$, where L is the perimeter and T the rotation period of the loop. The apparent radius R is approximated by $L/2\pi$. This technique has been also used for example in the North Atlantic by van Aken [2002] and Martins *et al.* [2002], in the North Pacific ocean by Rabinovich *et al.* [2002] and Takematsu *et al.* [1999], or by Lupton *et al.* [1998] to characterize subsurface hydrothermal plume in the eastern North Pacific.

[9] Owing to the relatively high spatiotemporal coverage, satellite altimetry provides an excellent opportunity to study mesoscale structures. However, to obtain better resolution, it is necessary to merge multisatellite altimeter data sets [Le Traon *et al.*, 1995, 1998; Ducet *et al.*, 2000]. Here, we use the gridded product of TOPEX/Poseidon (T/P), ERS-1/2, and Jason-1 sea level anomalies (SLA) provided by Archiving Validation and Interpretation of Satellite Data in Oceanography (AVISO). This data set spans the November 1992–March 2002 period with weekly SLA distributed on a $1/3^{\circ}$ Mercator grid. Sea level anomalies are relative to a 7 year mean calculated over the 1993–1999 period, and the spatial resolution varies between 30 km and 35 km in our study region. The mapping method used to process the data and reduced the errors are described in detail by Ducet *et al.* [2000]. The merged data set of T/P and ERS provides more homogeneous and reduced mapping errors than either

individual data set, yielding more realistic sea level and geostrophic current than the T/P data alone [Ducet *et al.*, 2000]. As the resolution of the gridded data is of order of 30–35 km in the region, and the SLA variations at 50 km wavelength have their energy reduced by 50% [Ducet *et al.*, 2000], this data set can be used to study eddies having diameters larger than 70 km, corresponding to the typical Rossby radius for the region [Chelton *et al.*, 1998]. Considering the geostrophic balance, residual sea surface velocity components were calculated from the SLA, using the geostrophic relation

$$U'_g = \frac{g}{f} \frac{\partial(\text{SLA})}{\partial y}$$

$$V'_g = -\frac{g}{f} \frac{\partial(\text{SLA})}{\partial x},$$

where g is the acceleration due to gravity, f is the Coriolis parameter, and ∂x and ∂y are the eastward and northward distances.

[10] Because we intend to identify only mesoscale eddies, the SLA maps were filtered to remove the low-frequency SLA variability associated, for example, with the El Niño Southern Oscillation events or with the seasonal cycle of the steric expansion/contraction. For each weekly map, we removed the mean SLA of the region, and we detrended the obtained data in both the zonal and the meridional directions. Figure 1c shows the original and the filtered SLA time series at the arbitrary chosen 11° S and 83° W position (black circle on Figure 1a). The large SLA of around 20 cm during the El Niño event of 1997–1998 and the seasonal SLA of -5 to -10 cm encountered each year in spring (September–October) disappear in the filtered time series. Figure 1d shows the spatially average spectrums of both the original and the filtered SLA series. It confirms that the interannual and annual energies are strongly reduced with this filtering method, but for the higher frequencies, relevant for this study, the form of the spectrum is unchanged. For commodity reason, hereinafter, SLA will denote the filtered SLA product.

[11] To identify eddies automatically, we used a criterion based on the SLA closed contours. The mean filtered SLA standard deviation is on average around 3 cm in the study region, varying from around 1.5 cm at 10° S to ~ 5 cm near the coast (not shown). For this reason, we adopt the ± 6 cm contour line in SLA as the edge of an eddy (around twice the mean standard deviation). Other relevant techniques of eddy identification can be found in the literature [e.g., Isern-Fontanet *et al.*, 2003; Morrow *et al.*, 2004], but many studies are based on SLA contour criteria. For example, Fang and Morrow [2003] and Morrow *et al.* [2004] used a 10 cm SLA to track eddies in the Indian and Southern oceans respectively; Wang *et al.* [2003] used a 7.5 cm criteria in the China Sea whereas a 5 cm contour has been used for the study of the Subtropical Countercurrent eddies [Hwang *et al.*, 2004]. For this study, we consider that all the ± 6 cm SLA closed contours determine the edge of an eddy. This choice, which is close to the 2–3 cm noise floor of altimetry [Le Traon and Ogor, 1998; Le Traon *et al.*, 1998],

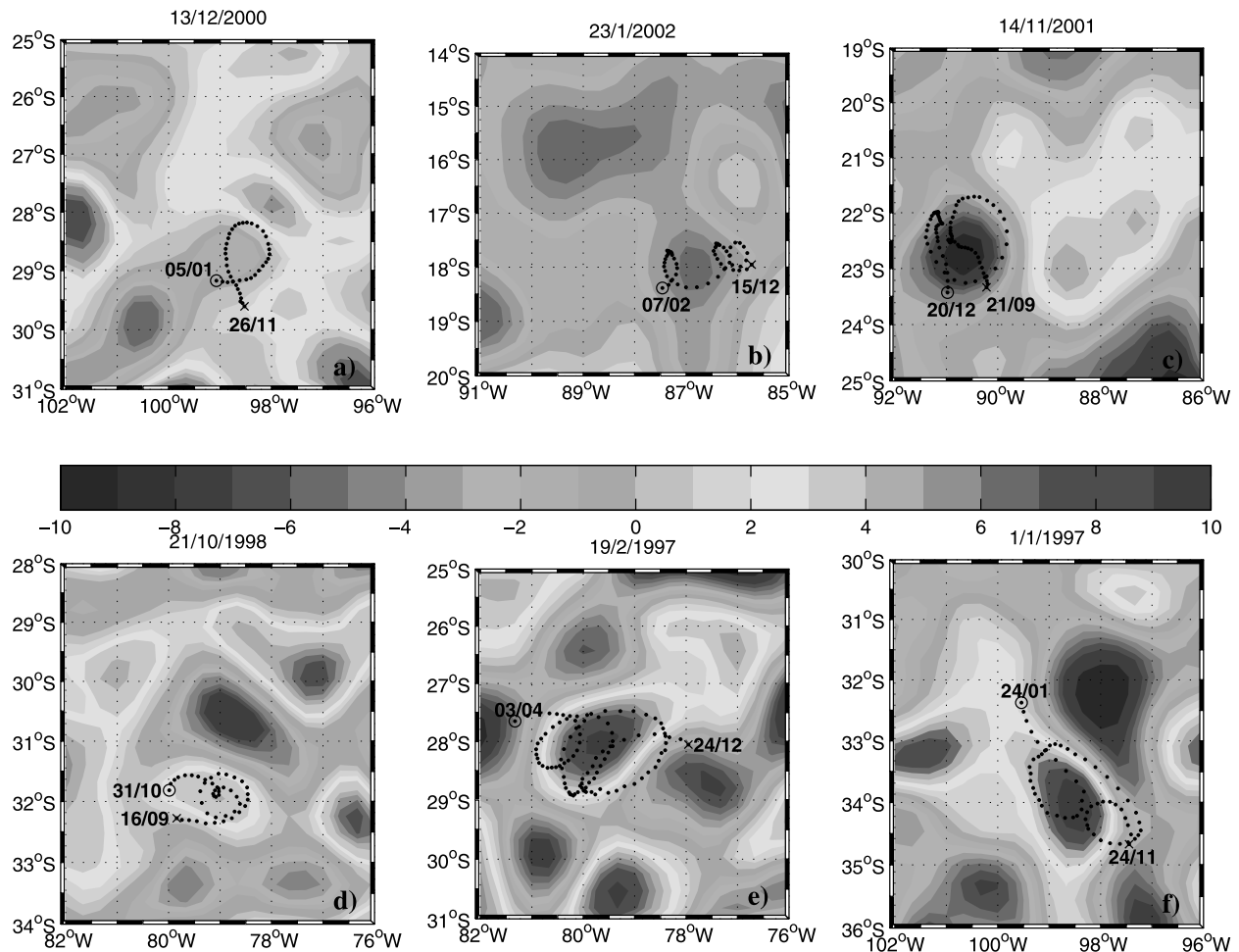


Figure 2. Examples of (a–c) cyclonic and (d–f) anticyclonic eddies identified from drifter data (black dots) and from sea level anomaly measurements (shading). The SLA are in centimeters. See color version of this figure at back of this issue.

eliminates the less energetic vortices. Center and apparent radius R were determined for each cyclonic (-6 cm) or anticyclonic eddy ($+6$ cm). Owing to the resolution of the altimetry gridded data, we do not retain eddies having a diameter lower than 70 km. The swirl velocity V_θ of each detected eddy is obtained by averaging the geostrophic velocities ($\sqrt{U_g^2 + V_g^2}$) on the corresponding ± 6 cm SLA contour. The rotation period of the eddy is then given by $T = 2\pi R/V_\theta$. Finally, we determine the eddy translation velocity V_T considering the distance between two consecutive positions of the eddy center.

[12] Satellite tracked drifters and merged altimetry measurements are well suited to mesoscale studies but are limited to the horizontal description. Complementary information on the vertical eddy structure can be obtained, however, from in situ data. For this goal, the last section of the paper will focus on a particular cold cyclonic eddy observed from the high-resolution WOCE P19 hydrographic section. This section was occupied in February–April 1993, principally from southern Chile to Guatemala along a nominal longitude of 88°W from 35°S to 20°S . Further north, it deflected eastward to 85.5°W (Figure 1a, black line). Between 35°S and 10°S a total of 54 deep conductivity-temperature-depth (CTD) sta-

tions were occupied by R/V *Knorr*, with spacing less than 50 km. The ship was also equipped with an Acoustic Doppler Current Profiler (ADCP), measuring velocity components from 30 m to around 450 m depth. The processing of the data, the vertical water properties, and the important features in the property distribution associated with the large-scale circulation can be found in the work of *Tsuchiya and Talley* [1998]. Here, we will concentrate on a cold and fresh mesoscale structure observed around 19°S and having a clear signature on the altimetry measurements.

3. Horizontal Eddy Characteristics and Statistics

3.1. Eddy Formation and Propagation

[13] Figure 2 shows examples of both cyclonic (Figures 2a–2c) and anticyclonic eddies (Figures 2d–2f) extracted from the daily drifter data. They are also clearly associated with mesoscale structures captured by altimetry measurements. Positive sea level anomalies are associated with anticyclonic eddies. Apparent loop diameters can vary from several kilometers (Figures 2b and 2d) to more than 150 km (Figure 2e), and the associated period of rotation varies from several days to more than one month. Some

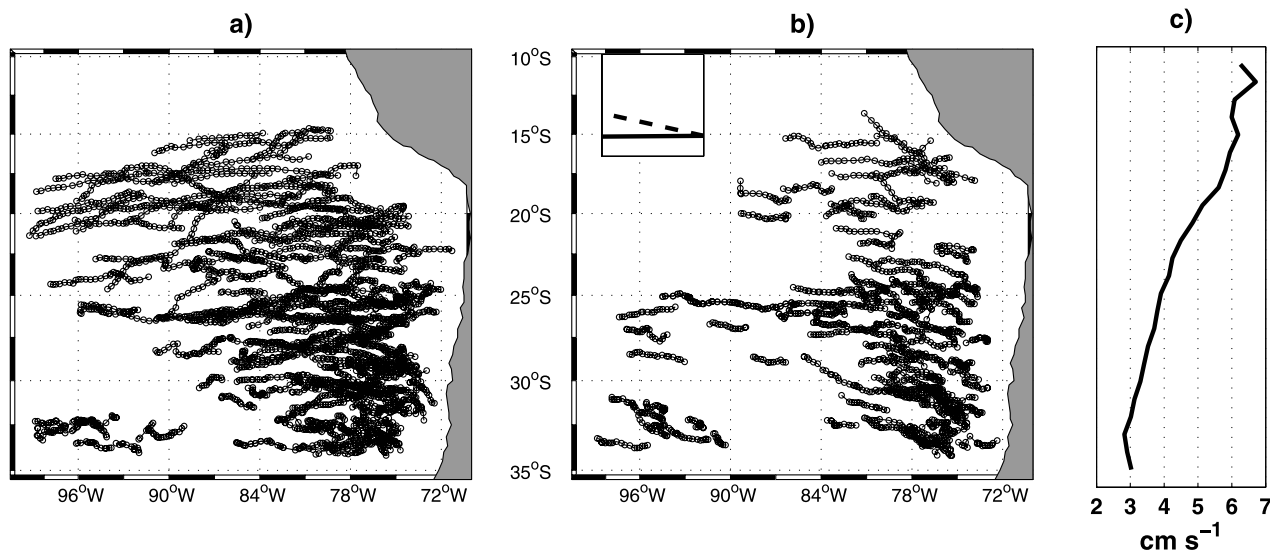


Figure 3. Propagation pathways for (a) cyclonic and (b) anticyclonic eddies tracked with altimetry data for more than 3 months. The inset in Figure 3b shows the mean propagation direction of the cyclonic (solid line) and anticyclonic (dashed line) eddies. (c) Mean translation velocity of the eddies as function of latitude.

eddies are more or less stationary but in general moving eddies are observed. Drifters can be “trapped” into an eddy observed by altimetry and moved with it for several weeks. During this mean advection, the drifting buoy shows different loops of the same rotation sense. Figure 2 also suggests that while the consecutive cyclonic loops are centered progressively westward or slightly south of due westward (Figures 2b–2c), the centers of consecutive anticyclonic loops move somewhat north of due westward (Figures 2e–2f). This is confirmed by the tracking of “long-lived” eddies, followed for more than 3 months from altimetry (Figure 3). Figure 3 shows that both cyclonic and anticyclonic eddies are principally generated near the coast where eddy kinetic energy (EKE) exhibits higher levels [Chaigneau and Pizarro, 2005]. The enhanced level of EKE and the formation of eddies near the coast, may be due to several processes, such as the interaction of the PCC system with the coastline, the strong upwelling front, or the intraseasonal and seasonal variability of the coastal flow [Pizarro *et al.*, 2002]. Furthermore, the intensification of the poleward subsurface Peru-Chile Undercurrent by the downwelling phase Kelvin waves can also destabilize the near surface coastal circulation [Shaffer *et al.*, 1997; Zamudio *et al.*, 2001] generating eddies. Eddies formed near the Chile-Peru Current tend to propagate either southwestward for the cyclonic vortices (Figure 3a) or northwestward (Figure 3b) for anticyclonic eddies. The inset Figure 3b shows the mean propagation directions for both the cyclones and anticyclones. It confirms that cyclonic eddies (solid line) move preferentially westward/southwestward with a mean angle of around $+0.4^\circ$ from the westward direction (positive for anticlockwise). In contrast, anticyclonic eddies (dashed line) propagate toward the northwest with a mean angle of -12.6° . This divergence in the warm and cold eddy pathways is linked to the β effect [Cushman-Roisin, 1994]: due to the rotation of the eddy, the surrounding water is advected to different latitude and so to a different planetary vorticity f . By conservation of potential

vorticity, it induces a change in relative vorticity on both flanks of the vortex. This β effect leads to a westward displacement for all eddies, but also to a poleward displacement of the cyclonic eddies, and an equatorward displacement of the anticyclonic vortices. This argument has been recently verified in the southeast Indian (Leeuwin Current eddies), in the southeast Atlantic (Agulhas eddies) and in the northeast Pacific oceans (Californian Current eddies) [Morrow *et al.*, 2004]. Here, we show that this propagation pattern is also observed in the eastern South Pacific region, for the Chile-Peru Current eddies. Figure 3c indicates that the translation velocity of the short and long-lived eddies increases equatorward from typical values of about 3 cm s^{-1} south of 30°S to around 6 cm s^{-1} north of 15°S . This northward increase of the translation velocity is consistent with the meridional changes of eddy motions on a β plane [Cushman-Roisin, 1994]. No significant difference was observed between the translation velocity speed of cyclonic and anticyclonic eddies. Furthermore, in contrast to the higher number of anticyclonic vortices identified from drifter data, Figure 3 indicates that there is 148 cyclonic and 90 anticyclonic long-lived eddies identified from the 10 years (1992–2002) of altimetry measurements. In general, long-lived anticyclonic eddies decay below the 6 cm s^{-1} level within 1000 km of the coast. Note, that Morrow *et al.* [2004] found that in the northeast Pacific, warm Californian Current eddies have a longer lifespan than their cyclonic counterparts, but their results were influenced by the strong El Niño event of 1997–1998 which was not filtered out from their altimetry data.

3.2. Eddy Characteristics

[14] The number of observed loops from drifters and altimetry provides a unique opportunity to characterize both the cyclonic and anticyclonic eddies in terms of period of rotation, swirl speed, apparent radius, and translation velocity. Figure 4 shows the cumulative functions of each eddy characteristic. The vortices observed from drifter data

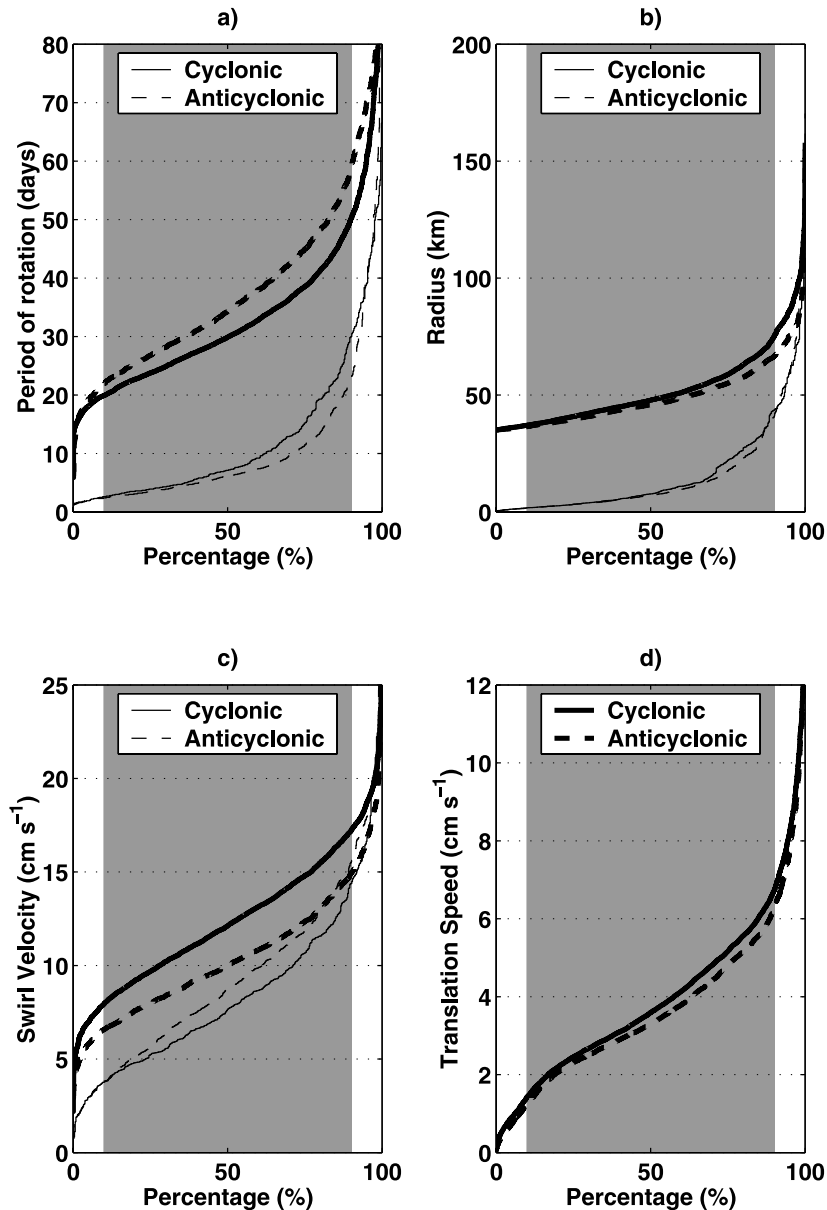


Figure 4. Cumulative functions of the eddy properties identified from drifter (thin lines) and altimeter data (bold lines): (a) rotation period, (b) radius, (c) tangential velocity, and (d) translation velocity. The 10–90% region is shaded.

and from altimetry show distinct rotation periods and associated radii: 90% of the 1290 eddies observed from drifter measurements have a rotation period lower than 25–30 days (Figure 4a) and a radius lower than around 40 km (Figure 4b); in contrast, 90% of the eddies observed from altimetry have a rotation period lower than 50–60 days and a radius in the range 35–75 km. The drifter measurements are thus important to characterize the small-scale loops unresolved by satellite data, whereas altimetry provides information on the larger scales. Ninety percent of the detected eddies have a swirl velocity lower than 15–17 cm s^{-1} (Figure 4c) and a translation velocity lower than 7 cm s^{-1} (Figure 4d).

[15] In order to study the radial evolution from the eddy center of the rotation period and tangential velocity,

Figure 5 shows the ensemble averages \bar{T} and \bar{V}_θ in different radius bins. Figure 5a shows that the rotation period increases outward quasi linearly for radii smaller than 100 km. For distance larger than 100 km from the eddy center, the time of rotation increases more strongly. Figure 5b shows that the tangential velocity increases rapidly over the first 20 km to a maximum of 14–15 cm s^{-1} at radii larger than 50 km. For radii larger than 100–120 km the swirl velocity estimated from altimetry slightly decreases (Figure 5b), associated with a change in the increasing rate of the rotation period (Figure 5a), and asymptotes to a 10–11 cm s^{-1} value. There is a good agreement between the drifter and altimeter results, but the tangential velocities obtained from drifter data are slightly higher. This can be linked to the neglected ageostrophic part

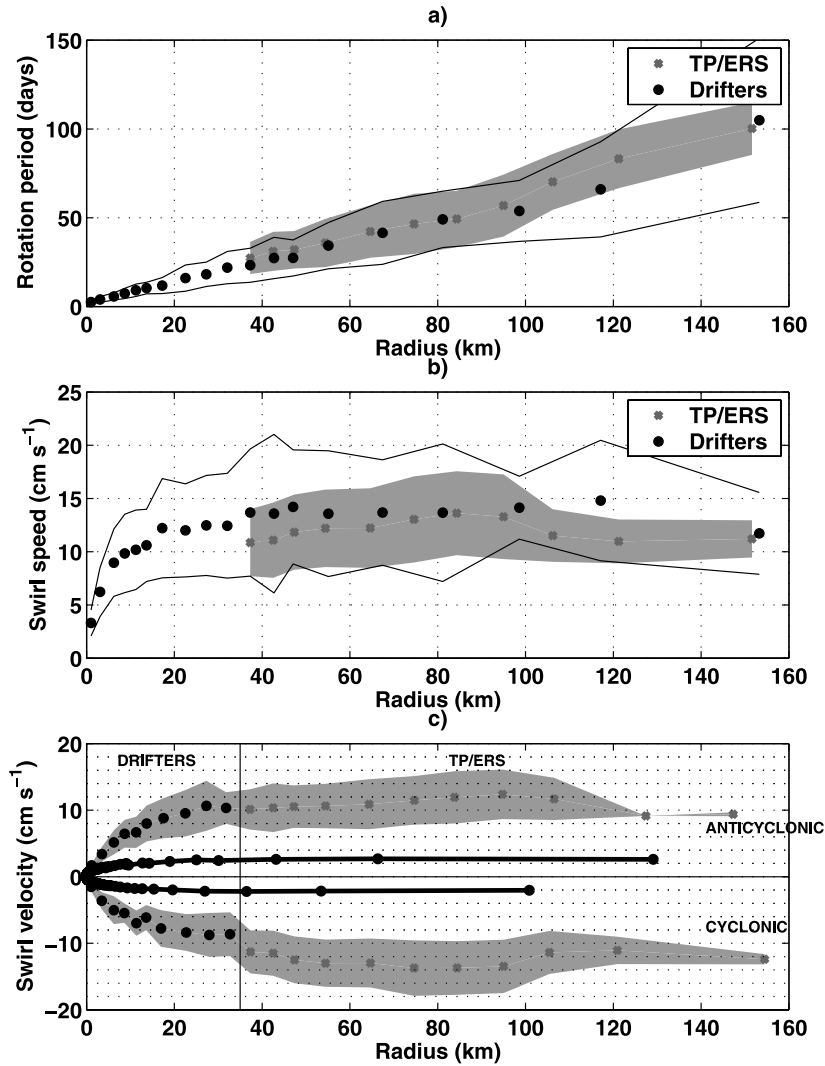


Figure 5. (a) Rotation period as function of the loop radius (= distance to the eddy center), based on all identified eddies from drifter (black dots) and altimetry measurements (shaded crosses). Black lines (shaded area) correspond to \pm one standard deviation around the mean value of drifter (altimetry) measurements. (b) Tangential velocity as function of loop radius. (c) Tangential velocity as function of loop radius for cyclonic ($V_\theta < 0$) and anticyclonic ($V_\theta > 0$) eddies. Drifter data are used for radii < 35 km, whereas satellite measurements are used for radii > 35 km. The shaded area corresponds to \pm one standard deviation around the mean value. Black dotted lines correspond to tangential velocities obtained from drifter rotary spectrum.

of the circulation in the altimeter measurements which can play an important role on the eddy kinetic energy [Chaigneau and Pizarro, 2005]. The discontinuity observed for radii larger than around 100 km may correspond to the critical size of the Chile-Peru Current eddies, quite close to the Rossby radius of around 95 km observed in the north of the region [Chelton *et al.*, 1998]. The corresponding swirl velocities of $14\text{--}15\text{ cm s}^{-1}$ are an order of magnitude higher than the observed translation velocities which vary from 3 cm s^{-1} to 7 cm s^{-1} from south to north of the study region (Figure 3).

[16] Do cyclonic eddies rotate more rapidly than anticyclonic vortices? Using drifter measurements for radial distance smaller than 35 km, and altimetry measurements otherwise, Figure 5c does not show clear differences between clockwise and counterclockwise vortices (Figure 5c), even if altimetry measurements suggest that cyclonic eddies have a

swirl velocity of around 2 cm s^{-1} higher than anticyclones (also shown in Figure 4c), this difference being in the range of the $3\text{--}4\text{ cm s}^{-1}$ standard deviation observed for all radius bins. In contrast, the tangential velocities directly deduced from the drifter rotary spectrum, show in absolute value, that the anticyclones rotate 30% more rapidly than the cyclonic vortices. However, these swirl velocities determined from the 63 trajectories longer than one year are an order of magnitude lower than the velocities determined previously. This reinforces the hypothesis that the choice of the closed loops and the $\pm 6\text{ cm SLA}$ contours discriminates the smaller, less energetic eddies. Furthermore, the rotary spectrum is influenced by others variabilities not directly associated with eddies such as filaments, current bursts, meanders.

[17] In this section we have studied the horizontal characteristics and some of the kinematic properties of cyclonic

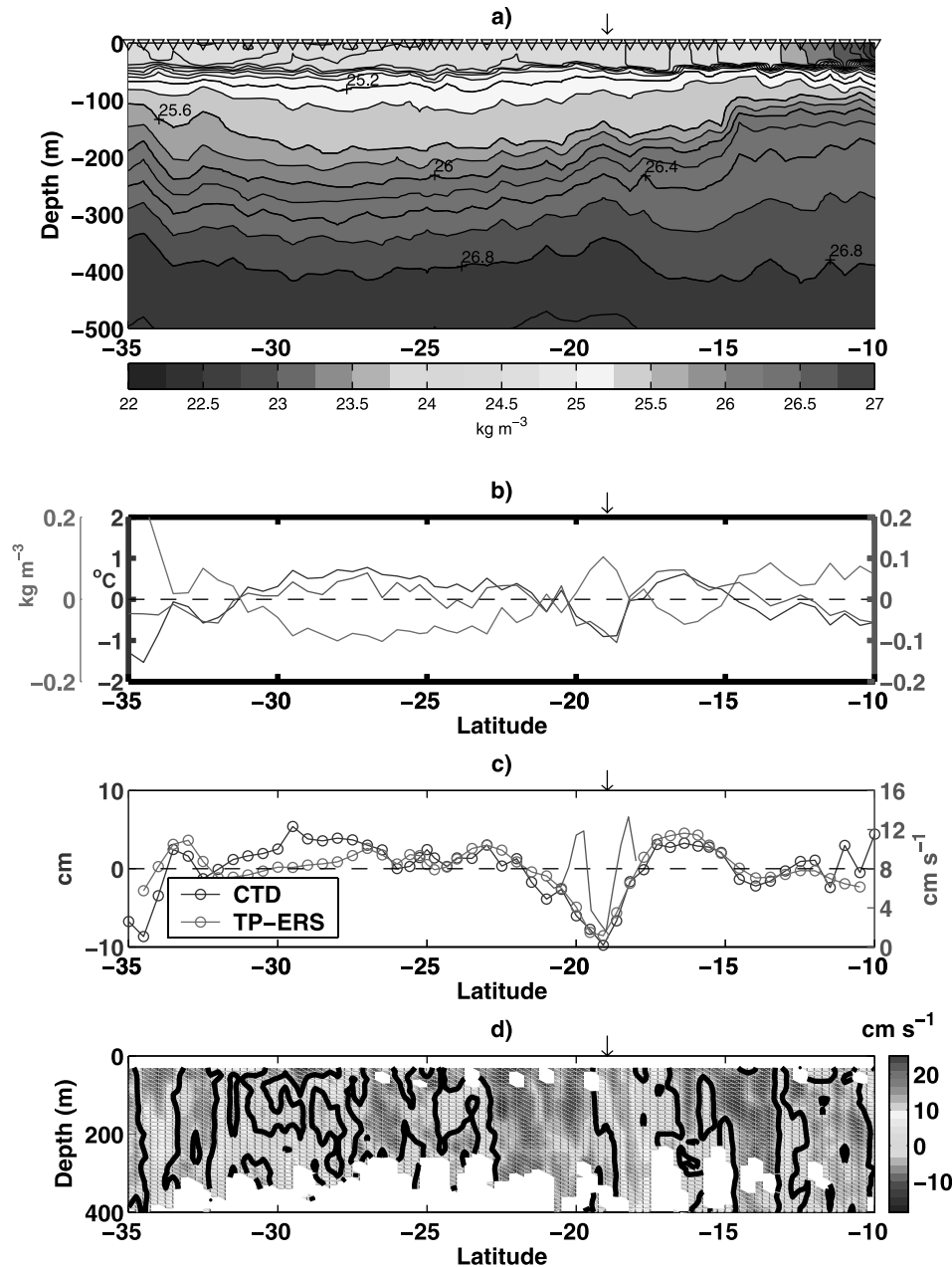


Figure 6. (a) Vertical distribution, over the first 500 m, of the potential density σ_0 along the WOCE-P19 section. (b) Temperature (blue), salinity (green), and density (red) averaged between 150 m and 500 m and detrended meridionally. (c) Dynamic height relative to 3000 m (detrended meridionally, blue), TP/ERS altimetry interpolated at the time and location of the WOCE-P19 measurements (red), and velocity from the ADCP data averaged between 30 m and 450 m (green). (d) Vertical distribution, over the first 400 m, of the zonal velocity from the ADCP measurements. Black arrows indicate the cold core eddy center position. See color version of this figure at back of this issue.

and anticyclonic eddies in the eastern South Pacific. In order to describe the vertical structure of the Chile-Peru Current eddies, the next section deals with a case study of a cold core eddy observed during the P19 WOCE section.

4. Vertical Eddy Characteristics: A Case Study of a Cold Core Eddy

[18] Figure 6a shows the vertical distribution, in the first 500 m of the water column, of the potential density obtained

from temperature and salinity CTD profile data during the P19 WOCE section between 35°S and 10°S. The properties of the different water masses and the effect of the large-scale circulation on the vertical tracer distributions are described in details in *Tsuchiya and Talley* [1998]. A particular mesoscale structure centered at around 19°S was sampled between the 18 and the 21 March 1993 (Figure 6a). The uplift of isopycnal levels at this latitude indicates the cyclonic nature of the eddy. The influence of this cold cyclonic eddy is visible down to 2000 m with a temperature

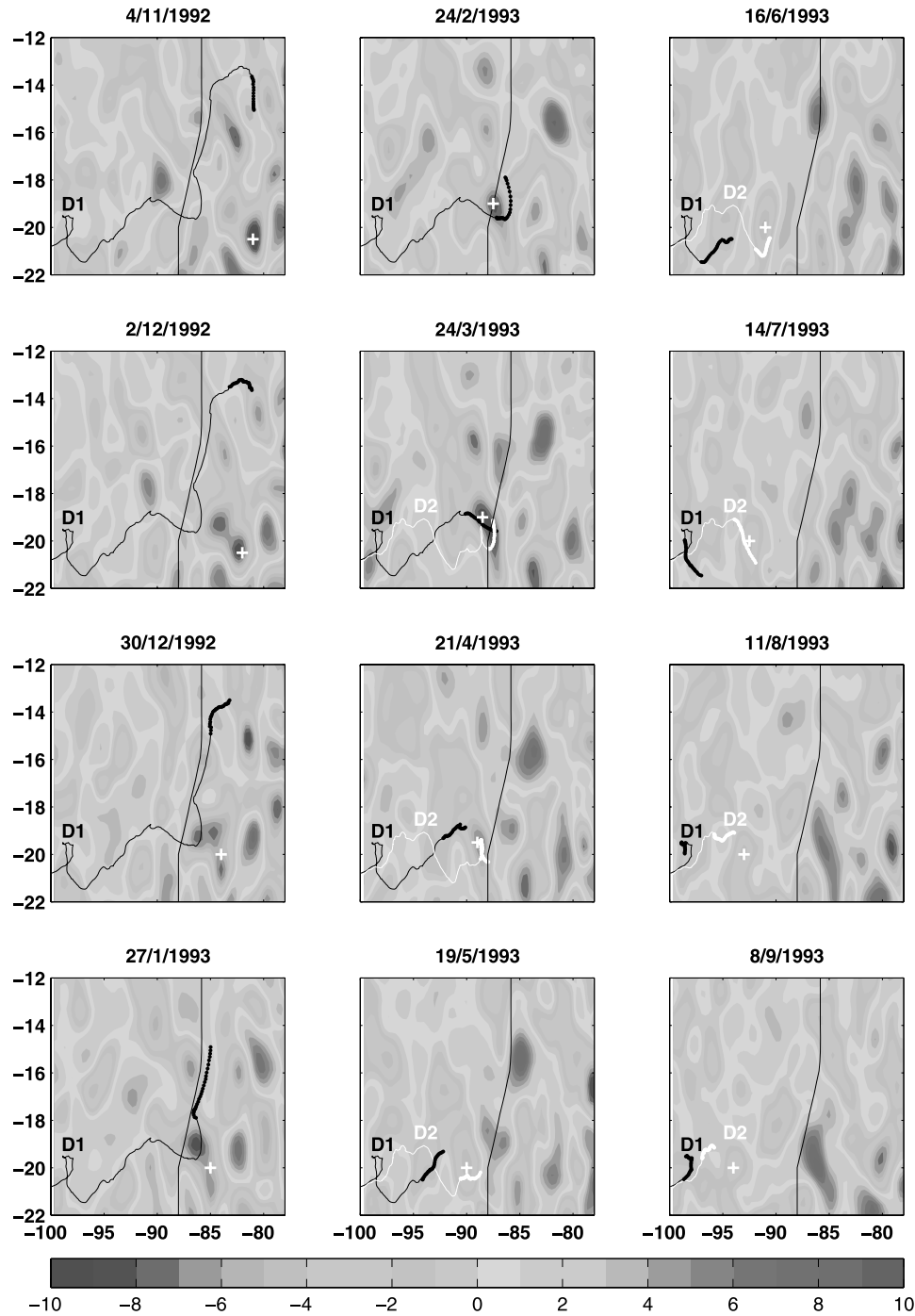


Figure 7. Time series of the SLA (in centimeters) between October 1992 and August 1993. The vertical solid line corresponds to the WOCE-P19 section. Drifter D1 (D2) track is shown by a black (white) line. The bold lines correspond to the drifter positions at the times of the SLA maps ± 14 days. The white crosses correspond to the cold core eddy position. See color version of this figure at back of this issue.

anomaly at this depth of around -0.1°C (not shown). In the absence of any other vertical hydrographic measurements of cold core eddy in the study region, we consider this depth (2000 m), as a typical vertical extension of the eastern South Pacific or Chile-Peru Current eddies. Figure 6b presents the temperature, salinity and density averaged over the 150–500 m layer and detrended meridionally. The cyclonic eddy centered at 19°S has a lower temperature of around 1° –

1.5°C and a lower salinity of around 0.1 – 0.15 compared to the surrounding water. This is associated with higher densities of around 0.1 kg m^{-3} . These anomalies can increase locally to more than -2.5°C in temperature and -0.4 in salinity. The northern and southern limits of the eddy are around 18°S and 20°S respectively corresponding to a radius approximately of 100 – 120 km . The surface data do not show important anomalies at 19°S (not shown). This

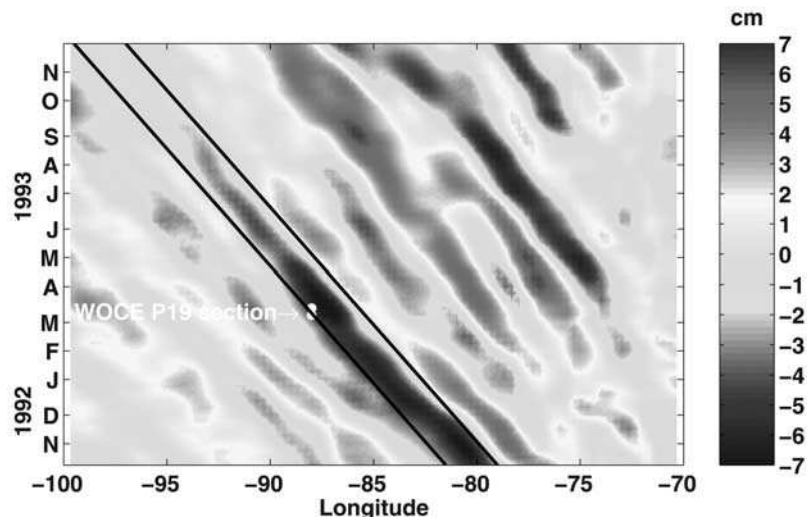


Figure 8. Longitude-time diagram of SLA averaged between 19° and 21°S. The white asterisks shows the moment when the WOCE-P19 stations between 19° and 21°S were occupied. See color version of this figure at back of this issue.

suggests that the eddy was formed far away from the WOCE section, and during its displacement toward the hydrographic section its surface properties were modified by air-sea exchanges (heat flux and evaporation/precipitation). As the air-sea interactions modify mainly the mixed layer properties at the scales considered here, below 150–500 m depth (and down to 2000 m) the eddy core may conserve the water properties of its formation region.

[19] Figure 6c (blue line) shows the dynamic height relative to 3000 m, calculated from in situ measurements and detrended meridionally. It compares quite well with the altimetry measurements interpolated along the WOCE section (red line). All along the section, the correlation is of 80% with 2 cm of rms difference; considering only the 15°–25°S latitude band, the correlation increases to 96% with 1.1 cm of rms difference. The cold core cyclonic eddy centered at 19°S exhibits a maximum sea level anomaly of around –10 cm. Near its centre, the velocity, corresponding to the ADCP measurements averaged between 30 m and 450 m, is of order of 2 cm s^{-1} (Figure 6c). This velocity increases toward the edges of the eddy to reach a maximum of 11.8 cm s^{-1} on the southern flank and 13.3 cm s^{-1} on the northern flank. The zonal velocity component (Figure 6d) is in agreement with the SLA slopes: south of the eddy centre, a negative meridional SLA gradient is associated with a negative (westward) zonal velocity, whereas north of the eddy core, the zonal velocity reverses eastward. As the eddy is well captured by SLA satellite measurements, we can trace it back in time to determine its formation region. Unfortunately, the satellite measurements began only the 14 October 1992, and we can follow the eddy only from this date. In beginning November 1992 the eddy was located at around 20.5°S and 81°W (Figure 7) and a second, weaker cyclonic centre is visible at around 19°S and 82°W. In December the two cyclonic eddies started to merge together. During the following months, this large –10 cm SLA centre propagated to the west and crossed the WOCE section from February to the end of March 1993, at the time

of the in situ measurements. From April, the cold core eddy lost its intensity and its SLA progressively reduced, but we can still track it visually until October 1993. On the basis of the –6 cm SLA contour, the apparent eddy radius at the time of the WOCE measurements is 102 km, in agreement with the estimated 100–120 km from in situ data (Figure 6). It confirms that the $\pm 6 \text{ cm}$ SLA contour is a robust criterion in the study region for the eddy edge identification. From Figure 5c, a cyclonic eddy of around 100 km wide may have a swirl velocity of around $12\text{--}13 \text{ cm s}^{-1}$ in agreement with the velocity estimated from ADCP data (Figure 6c).

[20] Figure 7 also shows that two different drifters have sampled this cold eddy. The first one (D1) was deployed at around 15°S and 80°W on 3 November 1992. It first flows North on the western flank of a cyclonic eddy (Figure 7b) before moving eastward and southward by different consecutive anticyclonic/cyclonic eddies. On 6 February 1993 it is trapped by the cold cyclonic eddy centered at 19°S and rotates at its edge during around 50 days. On the basis of these 50 days of daily displacements we estimate an independent eddy swirl velocity of 13.4 cm s^{-1} with a standard deviation of 6.2 cm s^{-1} . The second drifter (D2) where launched from the R/V *Knorr* at 19.1°S and 87.5°W the 20 March 1993. D2 is trapped in the eddy until mid-July 1993 but we only use its first 30 days of navigation to calculate the swirl velocity of the cold core cyclone. We estimate $V_0 = 12.2 \text{ cm s}^{-1}$ with a reduced standard deviation of 3.8 cm s^{-1} , in good agreement with both the velocity estimated from ADCP data and the calculations of the radial statistics given in the previous section. Finally, Figure 8 presents the longitude-time diagram of the SLA averaged meridionally on the 19°–21°S latitude band, for the October 1992–December 1993 period. Again, we see that the interesting cyclonic eddy was followed from 80°W in October 1992 to around 94°W in September 1993 with maximum amplitude of –8 to –10 cm until April–May 1993 after the crossing of the WOCE section. This eddy has thus traversed about 1500 km in an 11 months period, correspond-

ing to a translation velocity of around 5.2 cm s^{-1} , quite close to the mean V_T observed at this latitude (Figure 3c).

5. Discussion and Conclusion

[21] On the basis of satellite tracked drifter measurements, altimetry data, and in situ hydrographic section, this study has characterized the mesoscale structures and their propagation in the eastern South Pacific. We have highlighted the complementarities of these data sets: drifter data permit to study structures with radii smaller than 35 km that the multisatellite merged product does not resolve, whereas SLA measurements allow us to track eddies in time, and space hydrographic data are useful to have a vertical vision of the eddy cores.

[22] About 2/3 of the vortices identified from drifter data are anticyclonic, whereas 2/3 of the long-lived eddies tracked from altimetry measurements are cyclonic. Owing to its resolution and the applied optimum interpolation, the altimetry mapped data imposes certain space and time-scales. It misses a large part of the small-scale vortices and any ageostrophic convergence. In contrast, drifters are biased toward regions of convergent flow associated with anticyclones, higher velocities, and may give a biased representation of the entire eddy field (Figure 2). Thus open questions still remain such as, what part of the flow the altimetry signal represents? How the biased drifter movements can impact on our statistics? The higher number of drifter anticyclonic loops is due to the buoys trapping into convergent flow, or is it due to a cascade of the large-scale anticyclonic vorticity toward mesoscale motion? Further investigation, including high-resolution numerical simulations, is needed to respond to these questions. Even if the altimetry and drifter data measure different scales (Figure 4), the horizontal eddy size observed from altimetry data is in agreement with what observed in the interior ocean from hydrographic CTD measurements (Figure 6c). The smaller scales shown by the drifter loops may be influenced by ageostrophic components, more energetic near the surface.

[23] The majority of the long-lived eddies are formed near the coast in the Chile-Peru Current system where the EKE is higher [Chaigneau and Pizarro, 2005; Hormazabal *et al.*, 2004]. Then, they migrate westward in the direction of warmer and saltier offshore water, with a translation velocity of 3 cm s^{-1} south of 30°S to more than 6 cm s^{-1} north of 15°S . The higher number of cold cyclonic long-lived eddies can impact on the biology and biogeochemistry of the open ocean ecosystems [Siegel *et al.*, 1999]. Formation of cyclonic eddies in the coastal upwelling region uplifts nutrient-rich, isopycnal surfaces into the euphotic zone, where those nutrients are rapidly utilized by phytoplankton. In contrast, the downwelling associated with anticyclones pushes nutrient-depleted waters into the aphotic zone, where there is no ecosystem response [McGillicuddy *et al.*, 1998]. Thus the westward migration of the cyclonic eddies can influence the upper ocean biogeochemistry of the oligotrophic interior ocean. Furthermore, due to the β effect the meridional component of the translation velocity depends on the eddy rotation sense: cold cyclonic eddies migrate slightly poleward, whereas warm anticyclones propagate slightly equatorward. This divergence of the eddy pathways, which has been also observed

in others eastern boundary regions [Morrow *et al.*, 2004], may have important repercussions on tracer budgets, leading for example to a net equatorward heat transport. Finally, as the warm anticyclonic eddies move equatorward, they are subject in the southern hemisphere to a higher planetary vorticity; in order to maintain their absolute vorticity, their relative vorticity may decrease. Effectively, the relative vorticity of the anticyclonic “long-lived” eddies identified in Figure 3 decreases in average from $3.5 \times 10^{-6} \text{ s}^{-1}$ to less than $1 \times 10^{-6} \text{ s}^{-1}$ after 80 weeks of displacements (not shown). The associated standard deviation is around 10^{-6} s^{-1} . In contrast, the relative vorticity of the cyclonic long-lived eddies does not show important variation due the quasi westward motion of these cold cores.

[24] The critical extensions of the Chile-Peru Current eddies have appeared to be of order of 200 km laterally (radius of 100 km) and around 2000 m vertically. This large-scale eddies have in average a swirl velocity of around 14 cm s^{-1} and a rotation period of around 50 days. This tangential velocity is smaller than the 20 cm s^{-1} observed in the North Atlantic [van Aken, 2002] and than the $40\text{--}50 \text{ cm s}^{-1}$ of the more energetic Kuroshio region [Rabinovich *et al.*, 2002]. The mean radius of the loops observed from drifter measurements is around 10 km (Figure 4b). If we consider that the drifters are on average statistically evenly distributed on the eddy of radius R , the probability density $p(r, \theta)$ of finding the drifter at a radius r and direction θ relative to the centre of the eddy is constant and equal to

$$p(r, \theta) = \frac{1}{\int_0^R \int_0^{2\pi} r dr d\theta} = \frac{1}{\pi R^2}.$$

The mean distance $\overline{R_1}$, or the expectation

$$E(r) = \int_0^R \int_0^{2\pi} r^2 p(r, \theta) dr d\theta,$$

of the drifter from the eddy centre is then given by $\overline{R_1} = 2R/3$. A mean loop diameter of 20 km is thus associated with an eddy diameter of around 30 km, which corresponds to the typical mean diameter of the mesoscale Chile-Peru Current eddies. This order of magnitude is lower than the 30–95 km Rossby radii of deformation observed in the study region [Chelton *et al.*, 1998]. A typical eddy diameter of 30 km is also consistent with the Lagrangian length scales of 30–40 km observed in the domain [Chaigneau and Pizarro, 2005], but may depend of the considered latitude, since the Lagrangian length scales increase equatorward with the Rossby radius [Zhurbas and Oh, 2003, 2004].

[25] The swirl velocity structure of typical large eddy has been reconstructed from all the identified eddies. The radial distribution of the swirl velocity (V_θ as function of r) in eddies (Figure 5b) allows us to compare the relative and planetary vorticities (ξ and f respectively) using the relation [Pingree and Le Cann, 1992; van Aken, 2002]

$$\left| \frac{\xi}{f} \right| = \left| \frac{1}{f} \left| \frac{\partial(rV_\theta)}{r \partial r} \right| \right|.$$

At the critical radius of 100 km, the relative vorticity ξ is about 1% of f , suggesting that edges of large eddies are in geostrophic balance. The consideration of the geostrophic relationship to determine the swirl velocity at the eddy edges from altimetry measurements, appears then to be appropriate for large eddy diameters. The vorticity rate ($|\xi/f|$) of the eddies, increases when r decreases: at a radius of 10 km it is around 0.1 and around 0.4 near the centre. A relative vorticity of about 0.4 times the planetary vorticity suggests that eddy cores are ageostrophic. Although the large-scale eddies may be considered in geostrophic balance, ageostrophic dynamics and centrifugal effects may play an important role for the growth and decay of the mesoscale cores.

[26] Finally, these results could serve as a benchmark for interpreting and documenting the mesoscale activity in regional numerical models of the eastern South Pacific with regards to the choice of an appropriate spatial resolution. In that sense, this study may provide useful metrics for the validation of these high-resolution models along with help in developing strategies of future drifter deployments and cruise measurements.

[27] **Acknowledgments.** The drifter data were provided by the National Oceanic and Atmospheric Administration (NOAA). The authors thank Rosemary Morrow and Boris Dewitte for their helpful comments. A.C. was supported by ECOS-SUD and Fundación Andes grant D-13615. This work was also supported by the Chilean National Research Council (FONDAP-COPAS).

References

- Blanco, J. L., A. C. Thomas, M.-E. Carr, and P. T. Strub (2001), Seasonal climatology of hydrographic conditions in the upwelling region off northern Chile, *J. Geophys. Res.*, **106**, 11,451–11,467.
- Brugge, B. (1995), Near-surface mean circulation and kinetic energy in the central North Atlantic from drifter data, *J. Geophys. Res.*, **100**, 20,543–20,554.
- Chaigneau, A., and O. Pizarro (2004), Eddy characteristics and tracer transports from TP/ERS altimetry, in a region offshore Chile, *Proc. PORSEC*, **68**, 102–107.
- Chaigneau, A., and O. Pizarro (2005), Mean surface circulation and mesoscale turbulent flow characteristics in the eastern South Pacific from satellite tracked drifters, *J. Geophys. Res.*, **110**, C05014, doi:10.1029/2004JC002628.
- Chelton, D. B., R. A. deSzoeke, M. G. Schlax, K. El Naggar, and N. Siwertz (1998), Geographical variability of the first-baroclinic Rossby radius of deformation, *J. Phys. Oceanogr.*, **28**, 433–460.
- Cushman-Roisin, B. (1994), *Introduction to Geophysical Dynamics*, 320 pp., Prentice-Hall, Upper Saddle River, N. J.
- Ducet, N., P. Y. Le Traon, and G. Reverdin (2000), Global high-resolution mapping of ocean circulation from TOPEX/Poseidon and ERS-1 and -2, *J. Geophys. Res.*, **105**, 19,477–19,498.
- Fang, F., and R. Morrow (2003), Evolution, movement and decay of warm-core Leeuwin Current eddies, *Deep Sea Res., Part II*, **50**, 2245–2261.
- Hansen, D. V., and P.-M. Poulain (1996), Quality control and interpolations of WOCE-TOGA drifter data, *J. Atmos. Oceanic Technol.*, **13**, 900–909.
- Hormazabal, S., G. Shaffer, and O. Leth (2004), Coastal transition zone off Chile, *J. Geophys. Res.*, **109**, C01021, doi:10.1029/2003JC001956.
- Hwang, C., C.-R. Wu, and R. Kao (2004), TOPEX/Poseidon observations of mesoscale eddies over the Subtropical Countercurrent: Kinematic characteristics of an anticyclonic eddy and a cyclonic eddy, *J. Geophys. Res.*, **109**, C08013, doi:10.1029/2003JC002026.
- Isern-Fontanet, J., E. Garcia-Ladona, and J. Font (2003), Identification of marine eddies from altimeter maps, *J. Atmos. Oceanic Technol.*, **20**, 772–778.
- Jayne, S. R., and J. Marotzke (2002), The oceanic eddy heat transport, *J. Phys. Oceanogr.*, **32**, 3328–3345.
- Le Traon, P.-Y., and F. Ogor (1998), ERS-1/2 orbit improvement using TOPEX/Poseidon: The 2 cm challenge, *J. Geophys. Res.*, **103**, 8045–8057.
- Le Traon, P.-Y., P. Gaspar, F. Ogor, and J. Dorandeu (1995), Satellites work in tandem to improve accuracy of data, *Eos Trans. AGU*, **76**, 385–389.
- Le Traon, P.-Y., F. Nadal, and N. Ducet (1998), An improved mapping method of multi-satellite altimeter data, *J. Atmos. Oceanic Technol.*, **15**, 522–534.
- Lupton, J. E., E. T. Baker, N. Garfield, G. J. Massoth, R. A. Feely, J. P. Cowen, R. R. Greene, and T. A. Rago (1998), Tracking the evolution of a hydrothermal event plume with a RAFOS neutrally buoyant drifter, *Science*, **280**, 1052–1055.
- Martins, C. S., M. Hamann, and A. F. G. Fiúza (2002), Surface circulation in the eastern North Atlantic, from drifters and altimetry, *J. Geophys. Res.*, **107**(C12), 3217, doi:10.1029/2000JC000345.
- McGillicuddy, D. J., Jr., A. R. Robinson, D. A. Siegel, H. W. Jannasch, R. Johnson, T. D. Dickey, J. McNeil, A. F. Michaels, and A. H. Knap (1998), Influence of mesoscale eddies on new production in the Sargasso Sea, *Nature*, **394**, 263–266.
- Morrow, R., F. Birol, D. Griffin, and J. Sudre (2004), Divergent pathways of cyclonic and anti-cyclonic ocean eddies, *Geophys. Res. Lett.*, **31**, L24311, doi:10.1029/2004GL020974.
- Pingree, R. D., and B. Le Cann (1992), Three anti-cyclonic Slope Water Oceanic eDDIES (SWODDIES) in the Southern Bay of Biscay, *Deep Sea Res., Part A*, **39**, 1147–1175.
- Pizarro, O., G. Shaffer, B. Dewitte, and M. Ramos (2002), Dynamics of seasonal and interannual variability of the Peru-Chile Undercurrent, *Geophys. Res. Lett.*, **29**(12), 1581, doi:10.1029/2002GL014790.
- Poulain, P.-M., and P. P. Niiler (1989), Statistical analysis of the surface circulation in the California Current system using satellite-tracked drifters, *J. Phys. Oceanogr.*, **19**, 1588–1603.
- Rabinovich, A. B., R. E. Thomson, and S. J. Bograd (2002), Drifter observations of anticyclonic eddies near Bussol Strait, the Kuril islands, *J. Oceanogr.*, **58**, 661–671.
- Shaffer, G., O. Pizarro, L. Djurfeldt, S. Salinas, and J. Rutlant (1997), Circulation and low frequency variability near the Chile coast: Remotely-forced fluctuations during the 1991–1992 El Niño, *J. Phys. Oceanogr.*, **27**, 217–235.
- Siegel, D. A., D. J. McGillicuddy Jr., and E. A. Fields (1999), Mesoscale eddies, satellite altimetry, and new production in the Sargasso sea, *J. Geophys. Res.*, **104**, 13,359–13,379.
- Stammer, D. (1997), Global characteristics of ocean variability estimated from regional TOPEX/Poseidon altimeter measurements, *J. Phys. Oceanogr.*, **27**, 1743–1769.
- Stammer, D. (1998), On eddy characteristics, eddy transports, and mean flow properties, *J. Phys. Oceanogr.*, **28**, 727–739.
- Strub, P. T., J. M. Mesias, V. Montecino, J. Rutlant, and S. Salinas (1998), Coastal ocean circulation off western South America, in *The Sea*, vol. 11, edited by A. R. Robinson and K. H. Brink, pp. 273–313, John Wiley, Hoboken, N. J.
- Swenson, M. S., and P. P. Niiler (1996), Statistical analysis of the surface circulation of the California Current, *J. Geophys. Res.*, **101**, 22,631–22,645.
- Takematsu, M., A. G. Ostrovskii, and Z. Nagano (1999), Observations of eddies in the Japan Basin interior, *J. Oceanogr.*, **55**, 237–246.
- Tsuchiya, M., and L. D. Talley (1998), A Pacific hydrographic section at 88°W: Water property distribution, *J. Geophys. Res.*, **103**, 12,899–12,918.
- van Aken, H. M. (2002), Surface currents in the Bay of Biscay as observed with drifters between 1995 and 1999, *Deep Sea Res., Part I*, **49**, 1071–1086.
- Wang, G., J. Su, and P. C. Chu (2003), Mesoscale eddies in the South China Sea observed with altimeter data, *Geophys. Res. Lett.*, **30**(21), 2121, doi:10.1029/2003GL018532.
- Wunsch, C. (1999), Where do ocean eddy heat fluxes matter?, *J. Geophys. Res.*, **104**, 13,235–13,249.
- Zamudio, L., A. P. Leonardi, S. D. Meyers, and J. J. O'Bryen (2001), ENSO and eddies on the southwest coast of Mexico, *Geophys. Res. Lett.*, **28**, 13–16.
- Zhurbas, V., and I. S. Oh (2003), Lateral diffusivity and Lagrangian scales in the Pacific Ocean as derived from drifter data, *J. Geophys. Res.*, **108**(C5), 3141, doi:10.1029/2002JC001596.
- Zhurbas, V., and I. S. Oh (2004), Drifter-derived maps of lateral diffusivity in the Pacific and Atlantic Oceans in relation to surface circulation patterns, *J. Geophys. Res.*, **109**, C05015, doi:10.1029/2003JC002241.

A. Chaigneau, Centro de Investigación Oceanográfica en el Pacífico Sur-Oriental/Programa Regional de Oceanografía Física y Clima, Cabina 7, Universidad de Concepción, Concepción 3, Chile. (chaigneau@prof.udec.cl)

O. Pizarro, Departamento de Geofísica/Centro de Investigación Oceanográfica en el Pacífico Sur-Oriental/Programa Regional de Oceanografía Física y Clima, Cabina 7, Universidad de Concepción, Concepción 3, Chile. (orpa@prof.udec.cl)

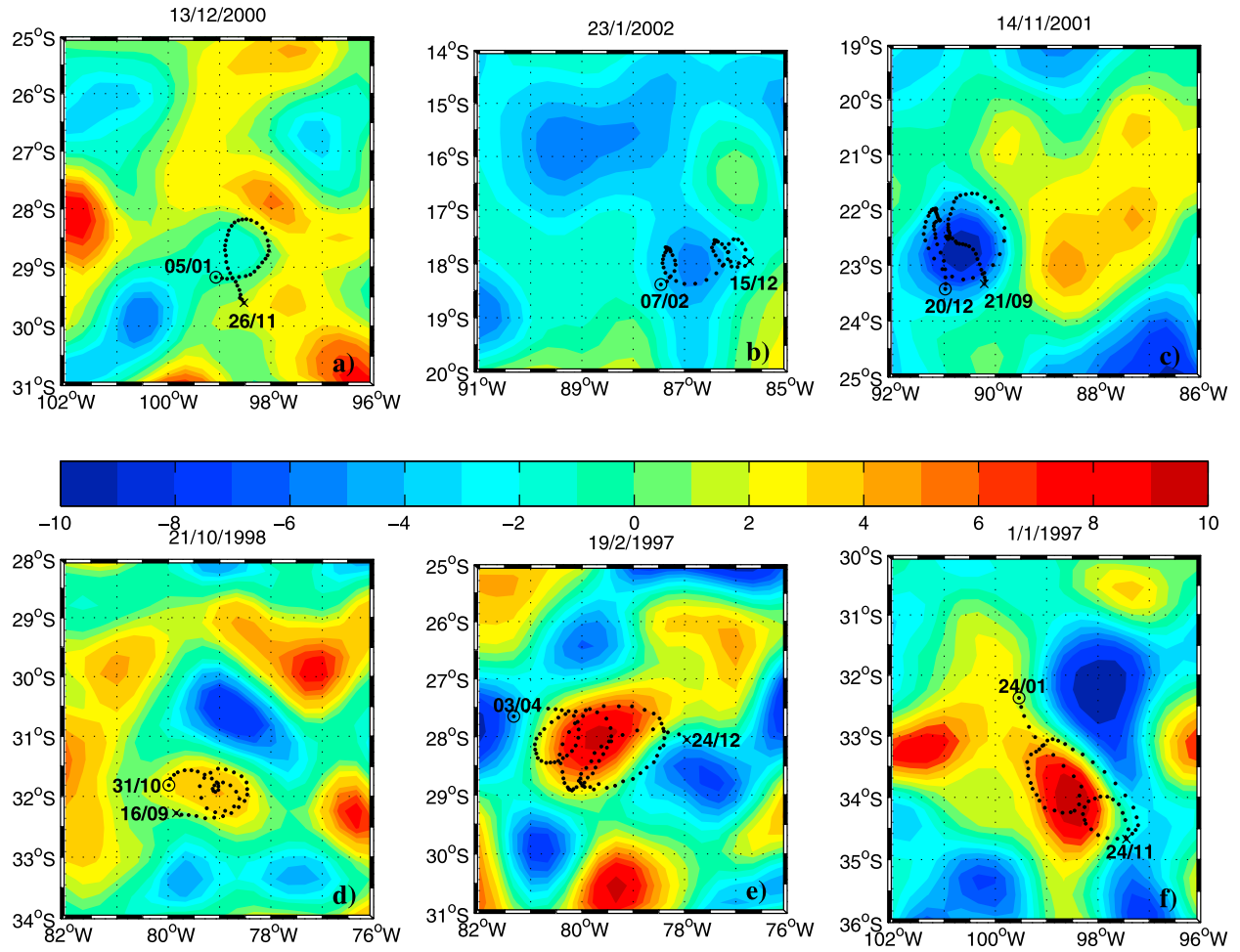


Figure 2. Examples of (a–c) cyclonic and (d–f) anticyclonic eddies identified from drifter data (black dots) and from sea level anomaly measurements (shading). The SLA are in centimeters.

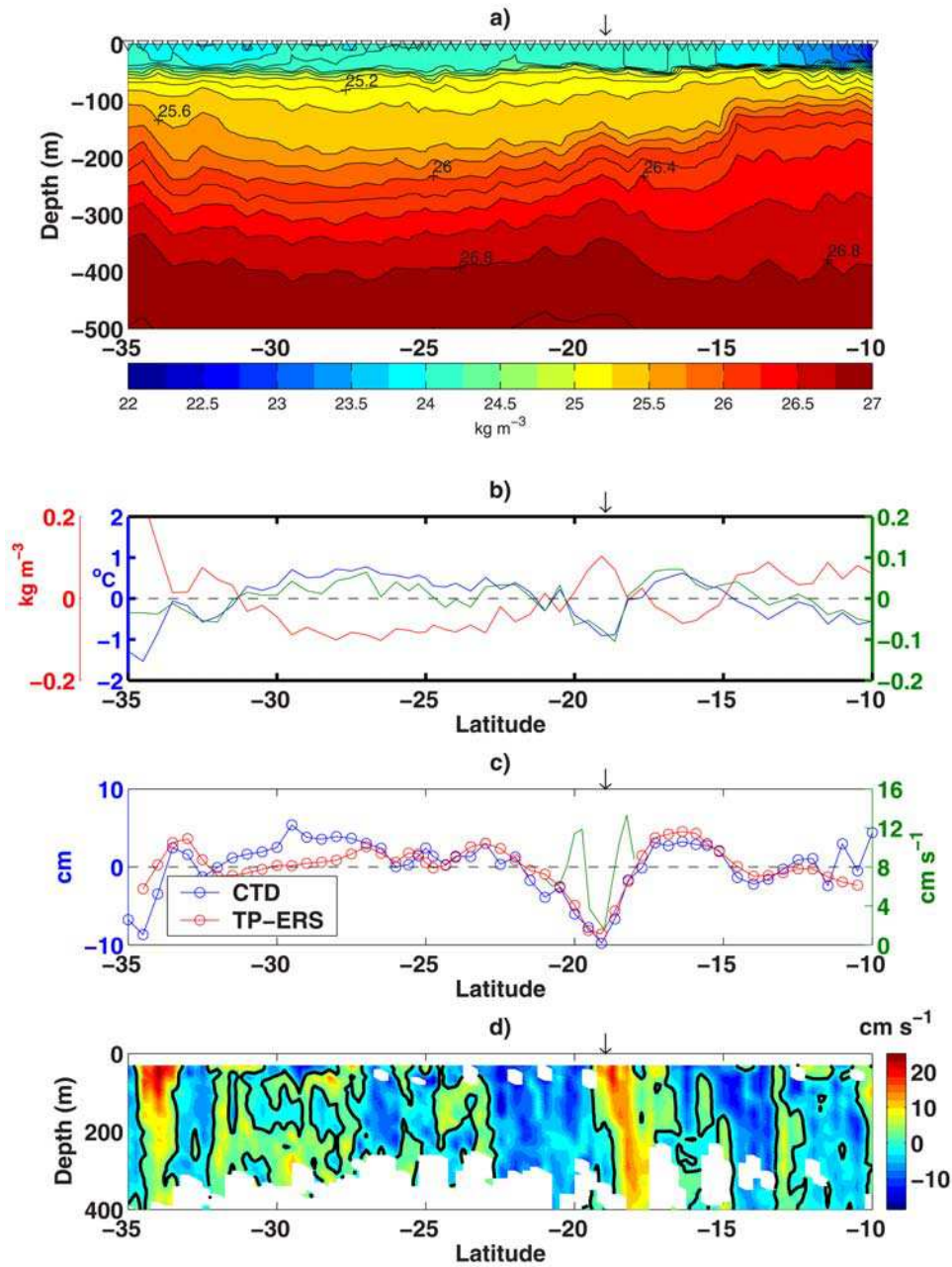


Figure 6. (a) Vertical distribution, over the first 500 m, of the potential density σ_0 along the WOCE-P19 section. (b) Temperature (blue), salinity (green), and density (red) averaged between 150 m and 500 m and detrended meridionally. (c) Dynamic height relative to 3000 m (detrended meridionally, blue), TP/ERS altimetry interpolated at the time and location of the WOCE-P19 measurements (red), and velocity from the ADCP data averaged between 30 m and 450 m (green). (d) Vertical distribution, over the first 400 m, of the zonal velocity from the ADCP measurements. Black arrows indicate the cold core eddy center position.

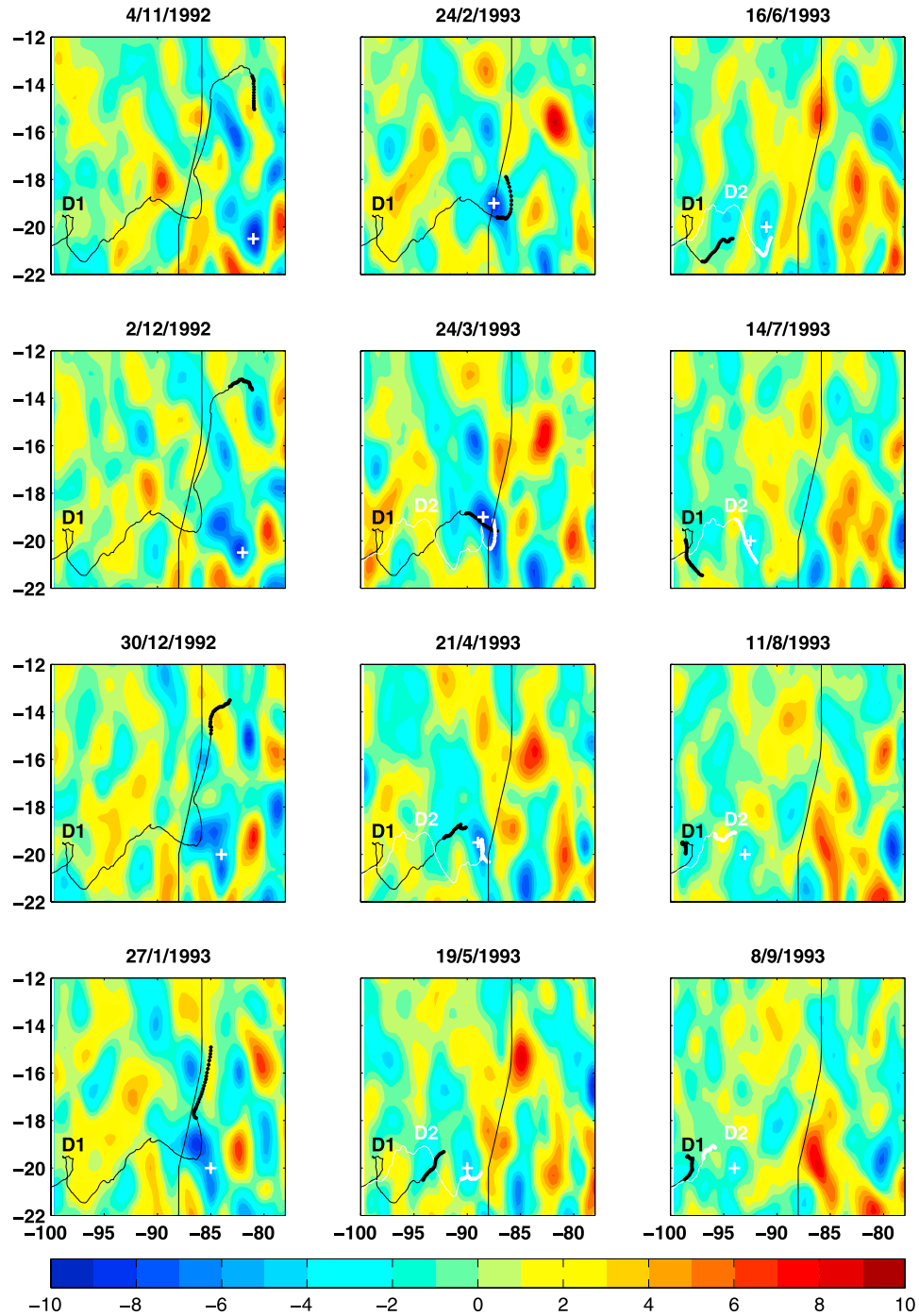


Figure 7. Time series of the SLA (in centimeters) between October 1992 and August 1993. The vertical solid line corresponds to the WOCE-P19 section. Drifter D1 (D2) track is shown by a black (white) line. The bold lines correspond to the drifter positions at the times of the SLA maps ± 14 days. The white crosses correspond to the cold core eddy position.

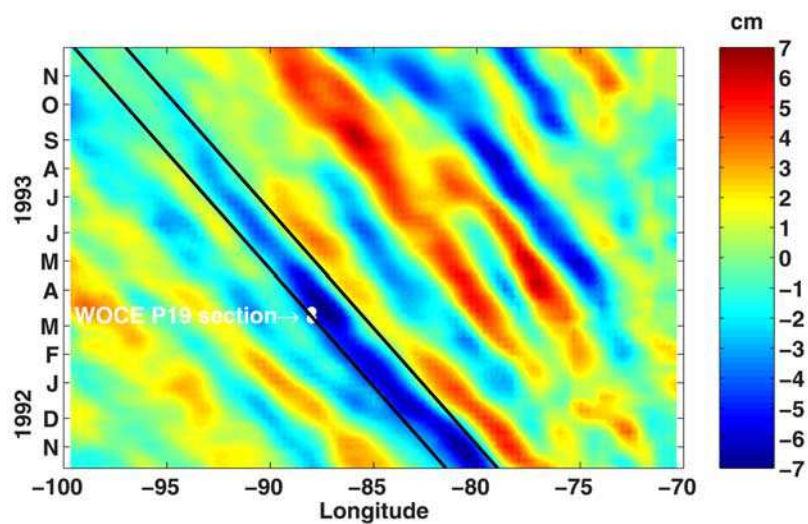


Figure 8. Longitude-time diagram of SLA averaged between 19° and 21° S. The white asterisks shows the moment when the WOCE-P19 stations between 19° and 21° S were occupied.